Dislocations in diamond: Electron energy-loss spectroscopy

C. J. Fall,[1] A. T. Blumenau,[1,2] R. Jones,[1,*] P. R. Briddon,[3] T. Frauenheim,[2] A. Gutiérrez-Sosa,[4] U. Bangert,[4] A. E. Mora,[5] J. W. Steeds,[5] and J. E. Butler[6]

[1]*School of Physics, University of Exeter, Exeter EX4 4QL, United Kingdom*
[2]*Theoretische Physik, Universität Paderborn, D-33098 Paderborn, Germany*
[3]*Department of Physics, University of Newcastle upon Tyne, Newcastle NE1 7RU, United Kingdom*
[4]*Physics Department, UMIST, Manchester M60 1QD, United Kingdom*
[5]*Department of Physics, University of Bristol, Bristol BS8 1TL, United Kingdom*
[6]*Code 6174, Naval Research Laboratory, Washington, DC 20375*

(Received 11 January 2002; published 15 May 2002)

Electron energy-loss (EEL) spectroscopy performed near dislocation cores is one of the few experimental techniques that can yield valuable information about the electronic levels associated with dislocations. In this study, we present experimental observations of low-loss EEL spectroscopy acquired on grain boundary dislocations in a CVD diamond film. We interpret these results using *ab initio* calculations, where we model low-loss and core-excitation EEL spectra acquired on various dislocation cores in diamond and compare them with bulk spectra. We consider in particular the 60° glide, 60° shuffle, and $\frac{1}{2}[110]$ screw dislocations, as well as the 30° and 90° partial glide dislocations and a 90° shuffle vacancy structure. The simulations show the absence of deep gap states for the more stable partial dislocations but there are characteristic changes to the low-loss EEL spectrum in the 6–12 eV region. Such changes are consistent with experimental spectra acquired from grain boundary dislocations found in boron doped CVD diamond.

DOI: 10.1103/PhysRevB.65.205206 PACS number(s): 71.55.−i, 78.20.Bh, 78.20.Ci

I. INTRODUCTION

The presence of dislocations in semiconductor crystals can strongly influence the electrical and optical properties of the material. In particular, the growth of polycrystalline chemically vapor deposited diamond generates high densities of dislocations (up to 10^{12} cm^{-2}), which originate in the substrate-interface region and can propagate throughout the thin film.[1] Such extended defects have notably been correlated with the so-called diamond band-*A* cathodoluminescence observed at 2.8–2.9 eV in undoped CVD diamond[2,3] and natural type-II diamond.[4,5] It has been noted that band-*A* luminescence is polarized with the electric field oriented parallel to the dislocation line,[4,5] and is associated with carbon atoms of reduced coordination.[3] Furthermore, it has recently been observed that color changes produced in natural brown diamonds by high-pressure, high-temperature annealing are linked to plastic deformations.[6]

The atomic structure of dislocations, and their dissociation into partials, has been widely studied experimentally in silicon and diamond by transmission electron microscopy (TEM).[7–9] However, this technique does not directly yield any information about the electronic structure of the dislocations. Spatially resolved electron energy-loss (EEL) spectroscopy performed near dislocation cores can in principle yield valuable information about electronic levels associated with dislocations, both within and above the band gap. Recent EEL experiments performed near extended defects in silicon[7] and diamond[10,11] have shown differences from bulk regions, but there are still issues regarding their interpretation. The information obtained from EEL spectroscopy could prove crucial to help resolve whether any electrical or optical activity is associated with undecorated dislocations.

In this study, we perform low-loss EEL measurements on a variety of dislocations in diamond and interpret these results using first-principles simulations of dislocation cores. By means of a simple model, we identify extended defect structures that lead to changes in EEL spectra compared with bulk regions. Furthermore, we find that some types of undecorated dislocations are consistent with observations of dislocation-related luminescence.

II. THEORETICAL FORMALISM

A. *Ab initio* method

The influence of structural defects on the electrical and optical properties of the material is determined essentially by the nature of the atomic bonding at the dislocation core. We perform self-consistent *ab initio* simulations of dislocation cores in diamond crystals within the local density approximation (LDA) to density functional theory, using the recently-enhanced AIMPRO code.[12] Local density functional theory is expected to give a realistic account of the ground state structure of the defects but it only gives an approximate description of excited states. In particular the energy gap is underestimated and both exciton and local field effects are ignored. In this sense the calculations described here are a first attempt to describe the EEL spectrum of dislocations.

The electronic wave functions are expanded in a set of *s*, *p*, and *d* atom-centered Gaussian orbitals with 28 variational degrees of freedom per atom. We use pseudopotentials to describe the ion cores.[13] A single dislocation, or partial dislocation, is placed within a hydrogen-terminated nanocrystal in a supercell, thus imposing perfect periodicity along the [110] dislocation core and describing dislocations of infinite length. The hydrogen atoms serve to terminate the surface bonds and avoid spurious surface states, but do not reflect a real physical presence. The advantage of this technique is

that a single infinite dislocation is modeled. A comparison between this approach and the normal one where a periodic array of dislocations is used is discussed in Ref. 14. Differences in the EEL spectra due to the different boundary conditions occur only at high energies well above the band edge. The atomic geometries of the dislocation cores have been presented in detail elsewhere.[15] The supercells used here contain between 60 and 160 atoms, and are fully relaxed to their equilibrium positions. We use between 2 and 4 Monkhorst-Pack reduced k points along the dislocation core to perform the Brillouin zone integrations during self-consistency.[16] Initial relaxations of the dislocation cores and estimates of the dislocation energies are performed using the density functional tight-binding method (DFTB),[17,18] with clusters of up to 600 atoms.[15]

B. Low-loss EEL spectroscopy

The low-loss part of the EEL signal results from the scattering of high-energy primary electrons with secondary valence electrons which undergo a transition to empty conduction or gap states. The signal obtained experimentally is representative of $-\mathrm{Im}\,\varepsilon(E)^{-1}$, where $\varepsilon=\varepsilon_1+i\varepsilon_2$ is the dielectric function and E is the energy loss.[19] We calculate the imaginary part of the dielectric function in the long-wavelength dipole approximation[20]

$$\varepsilon_2^l(E)=\frac{4\pi e^2}{\Omega}\sum_{c,v,\mathbf{k}}|\langle\Psi_{\mathbf{k}}^c|\mathbf{r}^l|\Psi_{\mathbf{k}}^v\rangle|^2\delta(E_{\mathbf{k}}^c-E_{\mathbf{k}}^v-E), \quad (1)$$

where Ω is the unit cell volume and $|\Psi_{\mathbf{k}}^{v,c}\rangle$ are valence and conduction states, with energies $E_{\mathbf{k}}^{v,c}$, respectively. The dielectric function depends only on the orientation of the electric field associated with the electron beam through the orientation of $\mathbf{r}$. Consequently, we compute EEL spectra for various orientations l of the electron beam. The sum over $\mathbf{k}$ includes the full Brillouin zone, which we sample with a regular Monkhorst-Pack grid containing 1000–5300 k points for bulk, and 50–150 k points for supercells. In a solid, the matrix elements of $\mathbf{r}$ must be evaluated using[21]

$$\langle\Psi_{\mathbf{k}}^n|\mathbf{r}|\Psi_{\mathbf{k}}^i\rangle=\frac{1}{i\omega m}\langle\Psi_{\mathbf{k}}^n|\mathbf{p}|\Psi_{\mathbf{k}}^i\rangle+\frac{1}{\hbar\omega}\langle\Psi_{\mathbf{k}}^n|[V_{nl},\mathbf{r}]|\Psi_{\mathbf{k}}^i\rangle, \quad (2)$$

where V_{nl} is the nonlocal part of the pseudopotential. The real part of the dielectric function is subsequently obtained through a Kramers-Kronig (KK) transformation, which then allows $-\mathrm{Im}\,\varepsilon(E)^{-1}$ to be computed. Low-loss EEL spectra are broadened using a Lorentzian function, which conveniently allows an analytical KK transformation.

More involved theories of dielectric functions have been developed for semiconductors, to describe effects beyond LDA,[22] beyond the long-wavelength limit,[23] and beyond the independent particle limit,[23,24] but they are currently too computationally intensive to be applied to anything other than bulk materials. It is difficult to be certain of the consequences of the omission of these effects. Moreover, experimental result will be affected by surfaces effects. Local field effects do not appear to be important for low momentum transfers.[25] Since we are interested in comparing bulk and defect-related EEL spectra, we restricted ourselves to the simple theory of dielectric functions presented above. To adjust the computed LDA band gap to the experimental value, the conduction bands are shifted upward by 1.48 eV. Gap states are shifted proportionally to their distance in energy from the top of the valence band.

C. Core-excitation EEL spectroscopy

Core-excitation EEL spectroscopy results from electronic transitions between deep core states and empty gap or conduction band states. In view of the localization of the initial state on an atom, core EEL spectra are related to an angular momentum projected local density of states on the atom. If the initial core state $|\Psi_{\mathbf{k}}^i\rangle$ is s-like (as for the diamond K edge), the core EEL spectrum from atoms at $\mathbf{R}$ is proportional to a p-projected local density of states at $\mathbf{R}$, written symbolically as

$$I_{\mathbf{R}}(E)=\sum_{c,\mathbf{R},\mathbf{k}}|\langle\Psi_{\mathbf{k}}^c|p_{\mathbf{R}}\rangle|^2\delta(E_{\mathbf{k}}^c-E_{i,\mathbf{R}}-E), \quad (3)$$

where $E_{i,\mathbf{R}}=E_a+\Delta V(\mathbf{R})$. $E_{i,\mathbf{R}}$ (E_a) is the core level for the solid (for the atom, respectively). To first order perturbation, $\Delta V(\mathbf{R})$ is the difference in potential at the atomic core between the bulk and the atom, and as a first approximation, we neglect its dependence on $\mathbf{R}$ in the following. The angular part of $p_{\mathbf{R}}$ is a Legendre polynomial of degree 1 while the radial part is taken to be of constant unit height in a shell of radius 1 a.u. around $\mathbf{R}$, and zero otherwise. Tests with different radii did not materially change the simulated core EEL spectrum. This procedure, albeit approximate, eliminates the need to reconstruct the core wave function of the final state. We include 8–10 inequivalent atoms neighboring the dislocation core in the sums over $\mathbf{R}$. This level of theory makes no account of final state effects, which should in principle include interactions between the excited electron and the hole. However, as we show below, it allows a qualitative understanding of EEL spectra, and permits comparisons between bulk and defect regions to be made. Core EEL spectra are displayed with a Gaussian broadening of 0.8 eV.

III. EXPERIMENTAL

The sample was prepared by ion thinning a membrane 0.84 μm in thickness of boron-doped polycrystalline CVD diamond. The sample was grown on a 3-in diameter {100} oriented silicon wafer using a commercial Astex HPMM 1.5 kW microwave plasma reactor with a B/C ratio of 1333 ppm in the gas phase. SIMS measurements on a similarly grown sample suggest a boron concentration around 2×10^{21} cm^{-3}. The wafer was first soaked in buffered hydrofluoric acid for 60 minutes to remove any native oxide and hydrogen terminate the surface. It was then subjected to a pre-treatment process involving first heating to 500 °C in 500 sccm hydrogen flow at 15 Torr (without plasma) to desorb all oxide species. Second, a thin carbonaceous layer was deposited at 800 °C using 30 min of 800 W microwave power at a pressure of 15 Torr and a hydrogen flow of 500 sccm and a

methane flow of 4 sccm. Third, the coated wafer was removed from the microwave reactor and put in a suspension of 5 g of 6–12 μm diamond powder in 600 ml of methanol and immersed in an ultrasonic bath for 30 min. It was then rinsed in methanol and blown dry with nitrogen. Finally the wafer was placed back into the reactor for diamond growth. The growth run took 9 h at 800 °C, 800 W, 15 Torr, 500 sccm hydrogen, 1.5 sccm methane, 2 ccm of a 0.1% mix of B_2H_6 in hydrogen. The growth rate and thickness were monitored near the center of the wafer using a 670 nm diode laser reflectometer.

After growth, the membrane was created by etching a 4–6 mm diameter hole from the back side of the silicon wafer using a mixture of hydrofluoric, acetic and nitric acids. A sample was prepared for TEM investigation using an argon/water vapor mixture in a Gatan PIPS ion thinner. As the B/C ratio in the reactants was 1333 ppm the sample was quite highly boron doped as confirmed by the deep blue color of the 0.84 μm thick film.

Plan view TEM examination of the ion thinned sample revealed a continuous film of polycrystalline diamond composed predominantly of grain clusters with a common $\langle 110 \rangle$ or $\langle 112 \rangle$ growth direction. The largest of these clusters were about 0.2 μm in diameter and they were internally twinned with $\{111\}$ twin contact planes parallel to the growth direction. Some were twinned on a single set of parallel planes. The larger grains were twinned in equivalent $\{111\}$ planes often with a fivefold node at the cluster center. Such $\langle 110 \rangle$ oriented clusters frequently contained up to ten or so individual grains in twin relationship with each other. Dislocations parallel to the growth direction were therefore predominantly $\langle 110 \rangle$ oriented.

Electron energy loss (EEL) spectroscopy was conducted in a VG 601, a cold field emission gun scanning transmission electron microscope (STEM), operated at 100 kV and equipped with a Gatan666 parallel EEL spectrometer. The EEL spectra of Fig. 1 were taken with an energy dispersion of 0.1 eV/channel. Subsequent low–loss spectra of dislocations were taken with a dispersion of 0.02 eV/channel in order to separate the low-loss spectrum from the tail of the zero loss peak. Thus data processing such as background removal via subtraction of an experimental zero loss peak, or via curve fitting, or deconvolution procedures was unnecessary. The accuracy with which the position of spectral features in the low-loss regime could be determined was ± 0.03 eV, while the energy resolution was slightly below 0.4 eV. Several tens of spectra were taken at each position with 1 s duration; they were then aligned and added. The electron probe size was 1 nm and the drift was less than 1 nm over several minutes, in fact it was undetectable over the time the spectra were taken. Surface contamination was removed by exposure to the electron beam before the EEL spectra were recorded.

IV. RESULTS

A. EEL spectra of diamond

The calculated EEL spectra are shown in Fig. 1, where we compare the low-loss and core-excitation spectra with the experimentally observed low-loss and core EEL spectra. Qualitative agreement between the computed and measured values is obtained and the peak positions are well described. The calculated and experimental spectra agree best below about 20 eV above which differences become significant. These may be due to the effect of surface plasmons or excitons. Absorption seen experimentally in previous core-loss spectroscopy in the band gap[10] may be attributed to surface effects or difficulties in background subtraction.

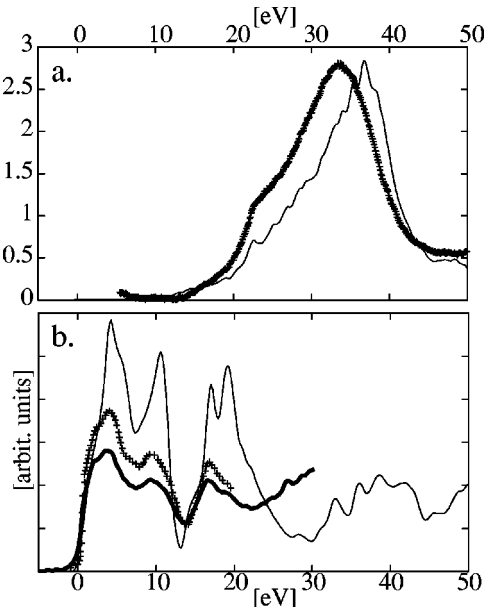

FIG. 1. Upper panel (a): Theoretical low-loss EEL spectrum of bulk diamond (solid line), compared with experimental data (crosses, this work). The experimental spectrum has been scaled to the same peak height as theory. Lower panel (b): Theoretical *K*-edge EEL spectrum of bulk diamond (thin solid line), compared with experimental data on type-IIb diamond from Bruley and Batson (crosses, Ref. 10) and on CVD diamond (thick line, this work). The experimental spectra have been arbitrarily scaled. The energy zero is set at the conduction band minimum, where the spectra have been aligned.

B. Theoretical EEL spectra of dislocations

In diamond, dislocations lie on $\{111\}$ planes and can be described by the angle between the dislocation line (parallel to a $[110]$ direction) and the Burgers vector. Glide and shuffle dislocations differ from each other in that the removed half-plane of atoms terminates after a long or a short inter-plane separation in the $[111]$ direction, respectively. 60° glide dislocations are known to dissociate into 30° and 90° partial dislocations separated by an intrinsic stacking fault (ISF).[8,26] Screw dislocations in diamond have also been observed to dissociate into partials.[9] Because shuffle dislocations can be obtained from glide dislocations by inserting (or equivalently removing) an extra row of atoms, several core structures of the dissociated shuffle dislocation are possible. Theoretical investigations using DFTB have shown that the following dissociation reactions into partial dislocations are energetically favorable:[15]

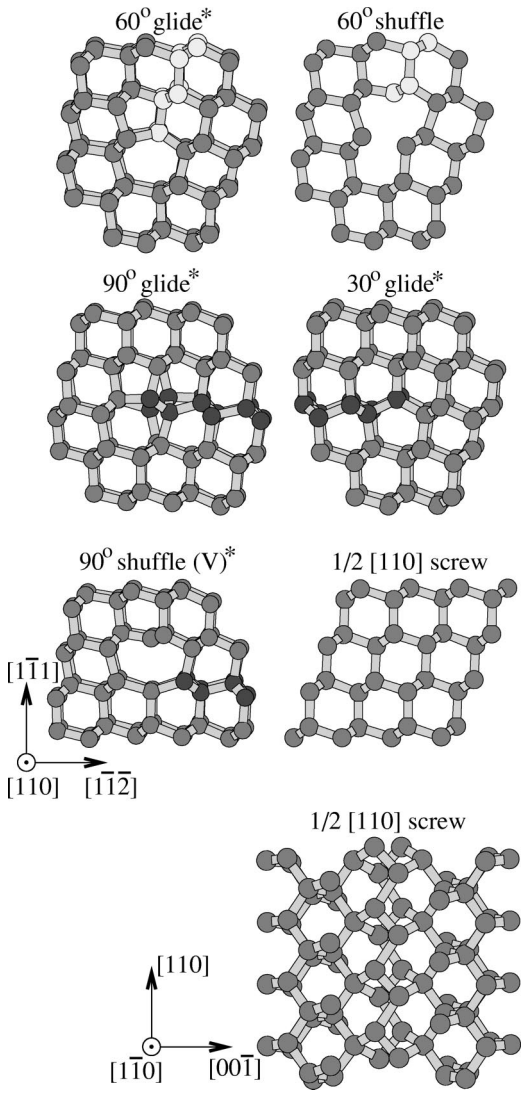

FIG. 2. Relaxed atomic structures of 60° glide and shuffle dislocations in diamond, as well as 30° and 90° partial glide dislocations. Also shown are a 90° shuffle vacancy structure [90° shuffle (V)] and a screw dislocation. The lower panel shows a side view of the screw dislocation. Only the central parts of the supercells used for relaxing the dislocations are shown. Lighter (darker) atoms indicate the stacking faults (inserted atoms, respectively). Asterisks denote structures with a double-period reconstruction in the [110] direction.

$$60° \text{ glide} \rightarrow 30° \text{ glide} + \text{ISF} + 90° \text{ glide},$$

$$60° \text{ shuffle} \rightarrow 30° \text{ glide} + \text{ISF} + 90° \text{ shuffle(V)},$$

$$\tfrac{1}{2}[011] \text{ screw} \rightarrow 30° \text{ glide} + \text{ISF} + 30° \text{ glide}.$$

The second reaction of course assumes the existence of the 60° shuffle dislocation even though it has a ~630 meV/Å higher core energy than the respective glide structure.[15] The atomic core structures of the dislocations listed above, relaxed with AIMPRO, are shown in Fig. 2. We consider in particular the 90° double-period partial dislocation, thought to be energetically favored over the single-period structure.[26]

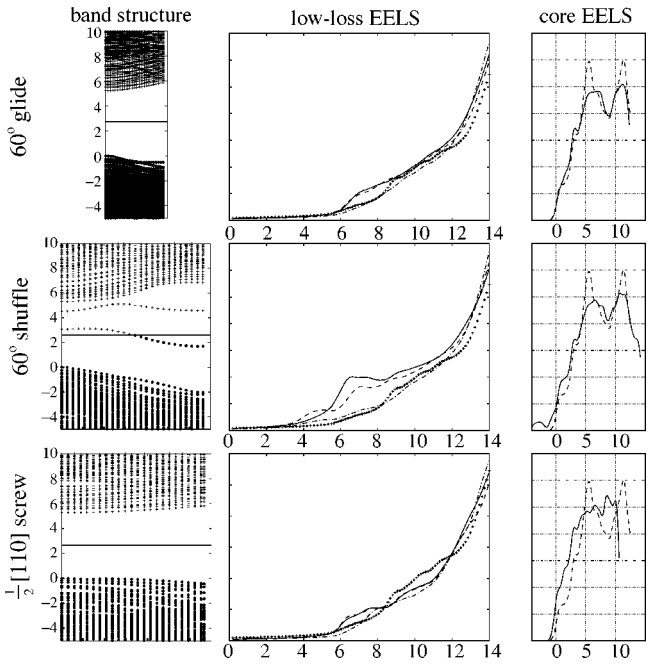

FIG. 3. Band structure along the dislocation core in the [110] direction in the gap region, low-loss EEL spectrum, and predicted *K*-edge core EEL spectrum for 60° glide, 60° shuffle, and $\frac{1}{2}$[110] screw dislocations corresponding to the atomic structures shown in Fig. 2. The double-period reconstructions fold the Brillouin zones (BZ) of some of the structures to half the thickness of the others. The BZ centers are on the left of each panel in the first column. In the band structures, the filled and empty states of neutral dislocations are separated by horizontal lines. The low-loss EEL spectra are shown for incident beams oriented in the $[1\bar{1}\bar{2}]$ (solid line) and $[1\bar{1}1]$ (dashed line) directions orthogonal to the dislocation axis, as well as along the [110] dislocation axis (dash-dot line), and are compared to superimposed bulk spectra superimposed (crosses). For core EEL spectroscopy, dislocation spectra (solid lines) are compared to bulk spectra (dashed lines). The energy zero set at the conduction band minimum in both cases. All energy scales are given in eV.

Many of these dislocation cores are reconstructed along the dislocation axis, thus lowering their energy by pairing dangling bonds. The 90° shuffle (V) partial is an open-core structure that can also be seen as a 90° glide core with one column of atoms removed. Further details about the structures are found in Ref. 15. We have studied the band structures, low-loss, and core-excitation EEL spectra of all these dislocation structures, and present the results in Figs. 3 and 4.

The 60° glide dislocation, as well as the 30° and 90° partial dislocations, show no evidence of gap states associated with undecorated dislocations, and only small changes in the corresponding low-loss and core-excitation EEL spectra compared with bulk. The lack of gap states stems from the reconstructed nature of the cores, which allow all the core atoms to be fourfold coordinated with bond lengths and bond angles similar to those of the bulk. The screw dislocation does not possess any deep gap states either, and has fourfold coordinated core atoms. Nevertheless, the band

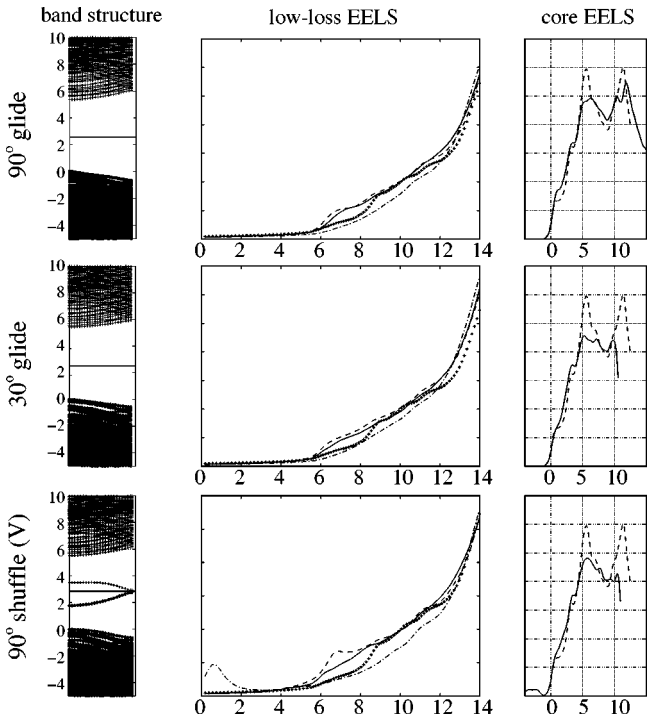

FIG. 4. Same as Fig. 3 for 90° glide, 30° glide, and 90° shuffle (*V*) partial dislocations.

structure is perturbed in the vicinity of the gap, leading to flatter band edges than seen in the bulk. The low-loss EEL spectra are suppressed for a beam parallel to the dislocation line in the 8–12 eV region, and enhanced for other orientations in the 6–8 eV region. A filling of the double peak observed in bulk at 6 and 12 eV above the conduction band minimum in the core EEL spectra is also found. This is related to the bond angles at the screw core (97°–126°), which are markedly different from those of the bulk (109.5°).

For diamond 60° shuffle dislocations and 90° shuffle (V) partials, we find evidence of empty states localized on the dislocation cores below the conduction band edge. These localized bands result from the undercoordinated carbon atoms at the dislocation core. For example, the gap states of the 90° shuffle (V) partial dislocation are formed from *p*-like orbitals of the threefold coordinated carbon atoms. Because of the double-period reconstruction, there are two gap states for each wave vector. In the lower gap state at $k=(0,0,0)$, the *p*-like orbitals are repeated along the core with a phase change of π between successive atoms, while in the higher gap state they are all in phase. Figure 5 shows the wave function of the localized state that is lower in energy. The 60° shuffle core additionally contains a stretched bond that contributes to an additional gap state that is higher in energy. Enhanced EEL absorption for the 60° shuffle is observed in the 3–12 eV range compared to bulk for beam orientations perpendicular to the dislocation axis. To compute the EEL signal of the 60° shuffle, which contains a half-filled band in the neutral state, we have assumed *p*-type conditions and empty gap states. For the open-core 90° partial, strong absorption in the 0–2 eV range is found for an electron beam

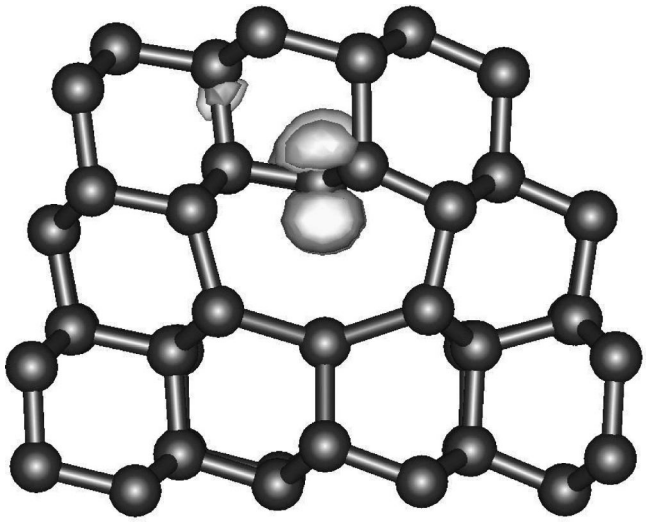

FIG. 5. Wave function associated with the gap state that is lower in energy (~1.8 eV above the valence band maximum) in a 90° shuffle (V) open-core partial dislocation at the Brillouin zone center. The wave function is centered on the threefold coordinated carbon atoms at the dislocation core. The figure is projected along the [110] direction, parallel to the dislocation axis.

oriented along the dislocation axis, and in the 6–9 eV range for a beam perpendicular to the dislocation axis. The presence of electronic bands around midgap is consistent with the observed energy of band-*A* emission at 2.8–2.9 eV, which has been correlated with threefold coordinated atoms in extended defects.[3] If core-excitation EEL is performed on these dislocations, the empty gap states create supplementary absorption peaks below the conduction band minimum. This could account for previous core-loss experimental findings.[10]

C. Experimental results

Due to the small grain size in the sample investigated, we were unable to determine by TEM the Burgers' vectors of those dislocations imaged in the STEM. We thus only state the direction of the dislocations with respect to the crystal and orientation of the electron beam.

Low loss spectra taken in nondislocated regions inside grains shown in Fig. 6 show a rise just after 6 eV with superposed weak undulations, followed by a steeper rise just after 12 eV, rather similar to the calculated bulk spectra (Figs. 3 and 4, crosses).

Most notable and easily identifiable in the TEM images were stacking faults and twin boundaries, some of them associated with strain and dislocations (Fig. 7), which because of the likeness to scenarios described in previous investigations on similar samples[27] were taken to be screw dislocations.

The experimental spectra of dislocations parallel to the electron beam appears generally more featureless and slightly less intense, when the low-loss intensity was normalized at an energy loss of 14 eV. However, bulk spectra taken at different locations, i.e., at different sample thicknesses or in different grains, show variations of similar strength. A comparison of the crosses and dash-dotted lines in Figs. 3

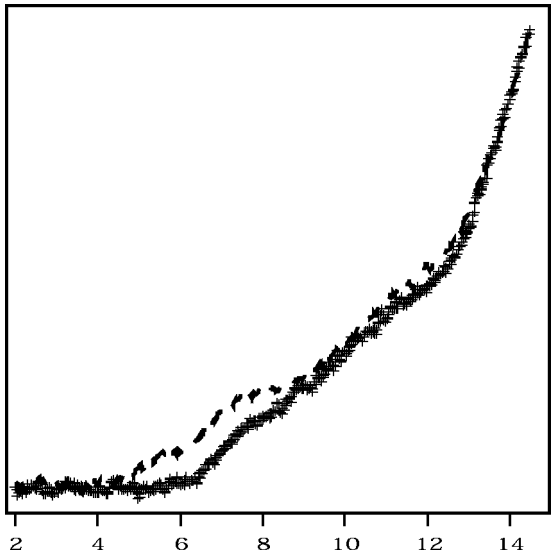

FIG. 6. Experimental low-loss EEL spectra for bulk (crosses) and oblique partial dislocation (dashed line) with electron beam along ⟨111⟩. Energy scale in eV.

and 4 demonstrates that the theoretical calculations also show that the spectra for electron beam incidence parallel to the dislocation line show small differences compared to the bulk spectra. The calculations suggest that much larger dislocation effects are expected when the electron beam is oblique to the dislocation line. Indeed, the calculated spectra in the 6–10 eV region obtained for electron beam incidence perpendicular to the dislocation line (full and dashed lines in Figs. 3 and 4) when compared with the bulk, suggest an additional loss in the 6–8 eV region.

Consistent with this is the experimental spectrum shown as a dashed line in Fig. 6, taken with the electron beam parallel to ⟨111⟩. This spectrum is due to a partial dislocation, presumably a dissociated screw, i.e., a 30° glide partial bounding a stacking fault. The dislocation line presumably lies along ⟨110⟩ and is oblique with respect to the beam direction. As it is neither perpendicular nor parallel to the electron beam, it does not directly correspond to any of the calculated spectra. It approximates the calculated dashed line for the 30° glide partial shown in Fig. 4 corresponding to an electron beam direction along ⟨111⟩ perpendicular to the dislocation line. The experimental spectrum shows a relative increase in the peak at 7 eV, similar to the calculated curve.

The peak at 7 eV occurs in all experimental spectra taken of dislocation lines oblique to the electron beam. This is in agreement with the calculations which show a relative increase of the shoulder around 7 eV as the most pronounced feature in all the dislocation spectra.

It should be emphasized that the relative intensities of the experimental spectra are expected to be different from those of the simulated spectra: the ratio of the bulk and dislocation volume in the experiment may vary between sampling points as the sample thickness varies; it is moreover generally larger than that used in the spectrum calculations. We have, however, demonstrated here that we are able to ascertain dislocation effects experimentally, and they prove to be in broad agreement with the theoretical predictions.

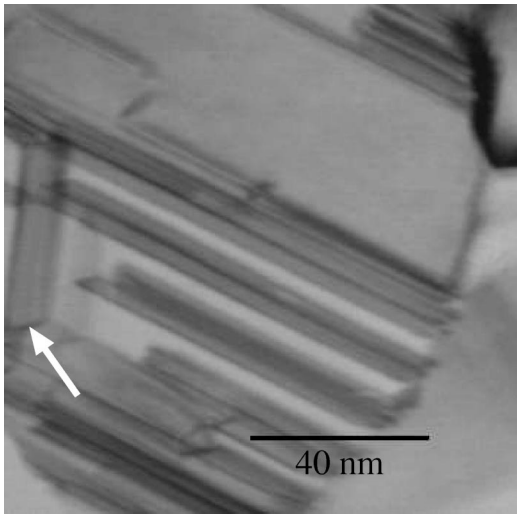

FIG. 7. TEM image of CVD diamond. The arrow marks the dislocation whose EEL spectrum is shown in Fig. 6.

V. SUMMARY

We have investigated the electronic structure of a number of dislocations in diamond. We find that the low energy 30 and 90° glide partial dislocations which border a (111) intrinsic stacking fault do not give rise to states in the band gap. Nevertheless, the calculated low-loss EEL spectrum of undecorated dislocations shows differences from bulk spectra. In particular, the spectrum taken when the electron beam is perpendicular to the line direction is expected to show the largest difference from bulk spectra with the onset moving to lower energies. Neutral shuffle dislocations give rise to a deep partially occupied band of gap states which leads to additional loss and is sensitive to the polarization of the electron beam. In the case of the 90° shuffle, a peak around 1–2 eV is found while the 60° shuffle dislocation leads to a strong peak around 6–7 eV for polarization perpendicular to the line.

The experimental low-loss EEL spectrum of bulk diamond is in substantial agreement with the calculated spectrum except that the onset is about one eV lower than the calculated spectrum. This might reflect the importance of excitonic effects.

Experimental EEL spectra have been acquired on partial dislocations bordering a stacking fault in boron-doped CVD diamond. Although it is likely that dislocations were contaminated with boron, their energy loss spectra show modest changes from bulk for an electron beam directed along the dislocation line, but supplementary loss in the 6–8 eV region for an electron beam oblique to the line. This is consistent with the theoretical spectra for screw dislocations derived from the glide set. No band gap absorption is detected experimentally. This suggests that the origin of band-*A* luminescence is either due to point defects, such as impurities or jogs, bound to dislocation lines, or to shuffle segments which have evaded detection by EEL spectroscopy.

ACKNOWLEDGMENTS

We thank R. Kalish and C. Cytermann (Technion) for carrying out the SIMS measurements.

*Electronic address: jones@excc.ex.ac.uk

[1] J.E. Graebner *et al.*, Phys. Rev. B **50**, 3702 (1994).
[2] J. Ruan, K. Kobashi, and W.J. Choyke, Appl. Phys. Lett. **60**, 3138 (1992).
[3] D. Takeuchi *et al.*, Phys. Rev. B **63**, 245328 (2001).
[4] I. Kiflawi and A.R. Lang, Philos. Mag. **30**, 219 (1974).
[5] P.L. Hanley, I. Kiflawi, and A.R. Lang, Philos. Trans. R. Soc. London, Ser. A **284**, 329 (1977).
[6] A.T. Collins, H. Kanda, and H. Kitawaki, Diamond Relat. Mater. **9**, 113 (2000).
[7] P.E. Batson, Phys. Rev. Lett. **83**, 4409 (1999).
[8] P. Pirouz *et al.*, Proc. R. Soc. London, Ser. A **386**, 241 (1983).
[9] W. Luyten, G. Van Tendeloo, S. Amelinckx, and J.L. Collins, Philos. Mag. A **66**, 899 (1992).
[10] J. Bruley and P.E. Batson, Phys. Rev. B **40**, 9888 (1989).
[11] H. Ichinose and M. Nakanose, Thin Solid Films **319**, 87 (1998).
[12] P.R. Briddon and R. Jones, Phys. Status Solidi B **217**, 131 (2000).
[13] G.B. Bachelet, D.R. Hamann, and M. Schlüter, Phys. Rev. B **26**, 4199 (1982).
[14] C.J. Fall, R. Jones, P.R. Briddon, A.T. Blumenau, T. Frauenheim, and M.I. Heggie, MRS Symposia Proceedings No. 693 (Materials Research Society, Pittsburgh, 2002), p. I10.1.
[15] A.T. Blumenau, M.I. Heggie, C.J. Fall, R. Jones, and T. Frauenheim, Phys. Rev. B **65**, 205205 (2002).
[16] H.J. Monkhorst and J.D. Pack, Phys. Rev. B **13**, 5188 (1976).
[17] D. Porezag, T. Frauenheim, T. Köhler, G. Seifert, and R. Kaschner, Phys. Rev. B **51**, 12 947 (1995).
[18] T. Frauenheim, G. Seifert, M. Elstner, Z. Hajnal, G. Jungnickel, D. Porezag, S. Suhai, and R. Scholz, Phys. Status Solidi B **217**, 41 (2000).
[19] D. Nozières and D. Pines, Phys. Rev. **113**, 1254 (1959).
[20] G. F. Bassani and G. Pastori Parravicini, in *Electronic States and Optical Transitions in Solids*, Vol. 8 of *International Series of Monographs in the Science of the Solid State*, edited by R. A. Ballinger (Pergamon Press, Oxford, 1975).
[21] A.J. Read and R.J. Needs, Phys. Rev. B **44**, 13 071 (1991).
[22] V. Olevano, M. Palummo, G. Onida, and R. Del Sole, Phys. Rev. B **60**, 14 224 (1999).
[23] W.R.L. Lambrecht and S.N. Rashkeev, Phys. Status Solidi B **217**, 599 (2000).
[24] L.X. Benedict *et al.*, Solid State Commun. **112**, 129 (1999).
[25] S. Waidmann, M. Knupfer, B. Arnold, J. Fink, A. Fleszar, and W. Hanke, Phys. Rev. B **61**, 10 149 (2000).
[26] R.W. Nunes, J. Bennetto, and D. Vanderbilt, Phys. Rev. B **58**, 12 563 (1998).
[27] J. W. Steeds, A.E. Mora, J.E. Butler, and K.M. Bussmann, Philos. Mag. (to be published).